High-resolution photoacoustic microscope for rat brain imaging in vivo

Xiaoquan Yang (杨孝全)[1], Xin Cai (蔡 鑫)[1], Konstantin Maslov[2], Lihong Wang (汪立宏)[1,2], and Qingming Luo (骆清铭)[1*]

[1] *Britton Chance Center for Biomedical Photonics, Wuhan National Laboratory for Optoelectronics, Huazhong University of Science and Technology, Wuhan 430074, China*

[2] *Optical Imaging Laboratory, Department of Biomedical Engineering, Washington University in Saint Louis, Saint Louis, 63130-4899, USA*

[*] *E-mail: qluo@mail.hust.edu.cn*

Received November 19. 2009

A reflection-mode photoacoustic microscope (PAM) for rat brain imaging *in vivo* is constructed. A pulsed laser is used as an excitation source, and a focused ultrasound transducer is adopted to collect the photoacoustic signal. Raster scanning is applied to acquire three-dimensional (3D) data. The obtained measurements of the lateral and axial resolutions of the microscope are 45 and 15 μm, respectively. The imaging depth in the chicken breast tissue is 3.1 mm at a signal-to-noise ratio (SNR) of 20 dB without any signal averaging. The imaging speed is 30 A-line/s. Experimental results *in vivo* demonstrate the capability of 3D imaging of the brain vessels of the rat after removing the skull.

OCIS codes: 180.0180, 170.0170, 110.0110.

doi: 10.3788/COL20100806.0609.

Brain imaging has been studied for many years due to its varied applications in disease diagnoses, neuronal activities observation, and brain research, etc. X-ray computed tomography (XCT), magnetic resonance imaging (MRI), and positron emission tomography (PET) have been widely used in this field[1]. Furthermore, optical imaging has been proven as an effective complementary modality due to the high correlation between optical signals and physiological activities[2]. However, the resolution of pure optical imaging is deteriorated by the scattering of photons in biological tissues. In addition, high-resolution optical imaging models, such as confocal and two-photon microscopy, are limited by the imaging depth of about 1 mm in tissues with high scattering coefficients[3,4]. Meanwhile, photoacoustic imaging uses photoacoustic waves based on thermoelastic expansion after the laser absorption of tissues[5,6]. It is a hybrid modality combining the high contrast of optical imaging and the low scattering of ultrasound imaging to break this limitation[7,8].

Three modes of photoacoustic imaging are normally used in biological tissues: transmission[9], reflection[10,11], and orthogonal modes[12,13]. Compared with the reflection mode, the transmission mode is limited by the thickness of the sample, while the orthogonal mode has worse axial resolution. In reflection-mode photoacoustic microscopy (PAM), both the vessels and the blood-oxygenation dynamics of mice brain are imaged[14,15]. Some photoacoustic imaging systems adopt ultrasound transducer (UT) arrays to accelerate imaging speed[16]. However, when time resolution is not the most critical issue, a single-element transducer with high central frequency and wide bandwidth is always used. This is because the transducer array with high central frequency is much more expensive and difficult to fabricate.

In this letter, we use a reflection-mode PAM to investigate the deep region in the brain of a rat. Spatial resolution, imaging depth, and imaging speed are presented. Three-dimensional (3D) imaging of a rat brain *in vivo* is also performed using the PAM.

The scheme of the system is shown in Fig. 1. A Nd:YAG laser (Surelite I-30, Continuum, USA) was used to provide 532-nm pulses with a duration of 6 ns and a repetition rate of 30 Hz. The laser was coupled into a multi-mode optical fiber after it was attenuated by a diffuser to prevent damage to the fiber. Laser output from the optical fiber was reshaped to an annulus using an axicon. It was then focused into the samples with dark-field mode. The focused laser spot was 3 mm in clear media, while the pulse energy of the laser induced into the sample was lower than 1 mJ. The laser density was set at about 14 mJ/cm^2 in order to fulfill the laser safety requirement for laboratory animals set by the National Institutes of Health (USA). A photodiode was used to measure the energy of each laser pulse for the necessary signal normalization due to poor laser stability.

The wide band focused UT (V30011, Olympus NDT, Japan), with a central frequency of 46 MHz and −6 dB bandwidth of 35 MHz, was used to collect ultrasound.

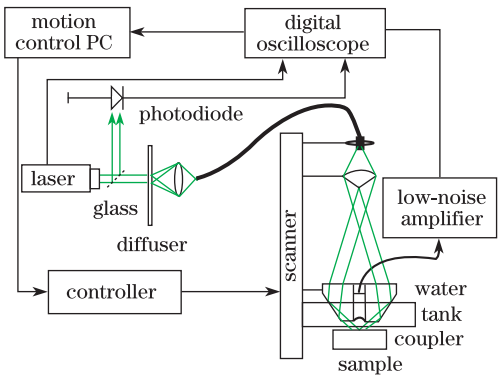

Fig. 1. Schematic of the PAM.

Using acoustic lens with a focal length of 6.7 mm, the UT achieved a high F-number of 1.03. It was fixed at the center of the condenser following the confocal adjustment of the condenser and the UT. The condenser with the UT was immersed into the water tank, which had a window at the bottom sealed with polythene membrane. The boundary was filled with ultrasonic coupler in order to avoid the reflection and diffraction of ultrasound at the boundary between the membrane and the sample caused by air bubbles.

The whole system worked under the control of laser pulses. The photoacoustic signal from the UT was amplified by a low-noise amplifier (ZFL-500, Mini-Circuits, USA) and then sampled by the oscilloscope (TDS5034B, Tektronix, USA), with a sampling rate of 250 MHz. The oscilloscope was triggered by the pulse which was synchronized with the laser. The digitalized data were stored in the oscilloscope for image reconstruction. At the same time, the pulse was sent to the motion control computer to transmit the command for starting a step motion of the scanner (WA100X100, Beijing Winneroptics, China). The raster scan was performed in a stepping-recording mode according to the parameters set by the user.

Since the focal spot of the incident laser is much bigger than that of the UT, the resolution of the system depends on the properties of the UT. The ultimate lateral resolution $\delta_{\rm l}$ of the UT is determined by the diffraction limit of the ultrasound with respect to the Rayleigh criterion. Since the UT is focused, it could be described as[17]

$$\delta_{\rm l} = 1.02c\frac{F}{f}, \tag{1}$$

where c is the velocity of the ultrasound in the sample, F is the F-number of the UT, and f represents the central frequency of the UT. The axial resolution $\delta_{\rm a}$ is affected by Δf, the bandwidth of the UT, and c[16] as presented by

$$\delta_{\rm a} = 2\ln 2 \times \frac{c}{\pi\Delta f}. \tag{2}$$

The resolution was measured using a carbon fiber with a diameter of 6 μm. The full-width at half-maximum (FWHM) values of the lateral and axial profiles of the carbon fiber were then measured as the resolutions. As shown in Figs. 2(a) and (b), the measured lateral and axial resolutions are 45 and 15 μm, respectively; in addition, the lateral resolution calculated with Eq. (1) using the parameters of the UT is 37 μm. The difference could be attributed to the pulse width of the laser and the shape of the sample. By analyzing the signal of the laser pulse with the Fourier transform, as shown in Fig. 3, we found that the pulse is a low-pass signal with –6 dB bandwidth of about 40 MHz. Therefore, photoacoustic signal could not provide enough high-frequency components and make the central frequency of the signal captured by the transducer lower. Furthermore, the ultrasound generated from the carbon fiber was a cylindrical wave, bringing phase distortion to a spherical focused transducer.

Although the resolution of the PAM beyond one mean-free path of photons can be improved using high-frequency UT, there is still a trade-off between imaging depth and resolution. The attenuation factor of the

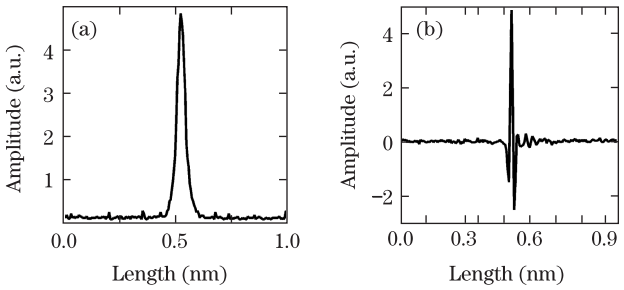

Fig. 2. Point spread function along the (a) lateral and (b) axial directions of the PAM.

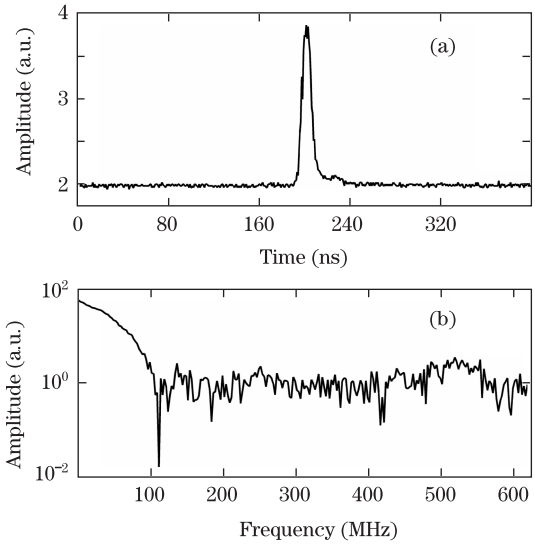

Fig. 3. (a) Signal of laser pulse measured with a photodiode (0.2 ns rising time) and (b) its Fourier transform.

50-MHz ultrasound signal used in our system is about 35 – 150 dB/cm in human skin[18], which is much higher than the optical attenuation coefficient of the 532-nm laser. Therefore, the imaging depth in the biological tissue of our system was determined through the high attenuation of the ultrasound signal. Black horse hairs inserted into a fresh chicken breast tissue were used to validate the imaging depth of our system. One horse hair was placed on the top of the tissue and another went through the same tissue slantwise. The upper black horse hair was used to indicate the position of the surface, while the lower one was used to estimate the signal-to-noise ratio (SNR) of the system at diferent imaging depths (Fig. 4). In this experiment, the position of the detector was adjusted to keep the focal zone of the UT at the middle of the two hairs. The horse hair embedded in the tissue was still visible at a depth of 3 mm, with the SNR of about 20 dB. The SNR can be potentially improved through signal averaging; however, with the current low pulse repetition rate laser, too much time would be consumed in the raster scan mode.

The pilot study of rat brain imaging with our system is demonstrated in Fig. 5. An adult, male Sprague-Dawley rat weighing 250 g was used. Separate doses of 0.2 g/kg a-chloralose and 1 g/kg urethane were administered intraperitoneally to anesthetize the rat before imaging. Afterwards, an imaging window of 7 × 4 (mm) was formed after the skull of one side of the parietal cortex was

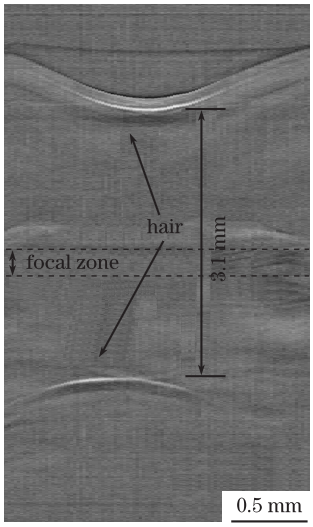

Fig. 4. Performance of the PAM at the depth of 3 mm by imaging two horse hairs embedded in a chicken breast tissue. The position of the focal zone of the transducer is indicated by the black dot lines.

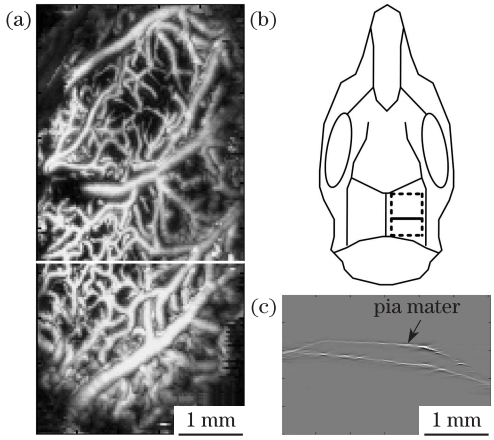

Fig. 5. Images of a rat brain captured with the PAM: (a) MIP of brain imaging; (b) scheme of a rat skull with indication of imaging window by dot lines; (c) B scan image of the rat's brain. The position is indicated by the white line in (a) and the black line in (b).

removed. The exact position is indicated by the dot lines in Fig. 5(b). During the imaging process, the rat was placed on a heat pad to maintain its normal body temperature. All the procedures done with the rat were in compliance with the Huazhong University of Science and Technology guidelines regarding the use and care of animals.

Figure 5 shows the result of the imaging of the rat brain using the PAM. In the imaging, the scanning area was 6×3 (mm), with an image matrix of 200×100. Considering the repetition rate of the laser, the total imaging time was about 15 min. The acquisition frequency of 250 MHz was adopted to utilize the bandwidth of the signal sufficiently. Therefore, with the acquisition data number of 500 at each position, a depth imaging scope of 3 mm was realized by taking into account the ultrasound speed of 1.5 km/s in soft tissues. Figure 5(a) is the maximum intensity projection (MIP) image of the rat brain imaging using the PAM. The projection was done along the depth direction, indicating that the maximum amplitude of the photoacoustic signal in each A scan was projected to the image at the position of A scan acquisition. The MIP image revealed the microvasculature on the cortex of the rat. For the PAM resolution of 45 μm, the diameters of vessels are wider than their real sizes. Figure 5(c) is a B scan image, with its position indicated by the white line in Fig. 5(a) and the black line in Fig. 5(b). It can be seen that the pia mater could be imaged using the PAM, and that the vasculature on the pia mater could be distinguished on the cortex.

In conclusion, a high-resolution PAM system for brain imaging of small animals *in vivo* is developed. The resolution, imaging depth, and imaging speed are measured. The *in vivo* study suggests that the PAM is suitable for brain imaging of small animals. However, its functionality is restricted by the wavelength of the laser. A multi-wavelength system is under construction, which could reveal much more information about the brain in future studies.

This work was supported by the National Natural Science Foundation of China (No. 60828009) and the Programme of Introducing Talents of Discipline to Universities (111 Project).

References

1. R. Cabeza and L. Nyberg, J. Cognit. Neurosci. **12,** 1 (2000).
2. Z. Wang and Q. Liu, Prog. Biochem. Biophys. (in Chinese) **35,** 488 (2008).
3. M. D. Cahalan, I. Parker, S. H. Wei, and M. J. Miller, Nat. Rev. Immunol. **2,** 872 (2002).
4. F. Helmchen and W. Denk, Nature Methods **2,** 932 (2005).
5. M. Xu and L. V. Wang, Rev. Sci. Instrum. **77,** 041101 (2006).
6. G. J. Diebold, T. Sun, and M. I. Khan, Phys. Rev. Lett. **67,** 3384 (1991).
7. C. Li and L. V. Wang, Phys. Med. Biol. **54,** R59 (2009).
8. L. V. Wang, Nature Photon. **3,** 503 (2009).
9. H. Zhang, Z. Tang, Y. He, and L. Guo, Rev. Sci. Instrum. **78,** 064902 (2007).
10. D. Yang, D. Xing, Y. Tan, H. Gu, and S. Yang, Appl. Phys. Lett. **88,** 174101 (2006).
11. H. F. Zhang, K. Maslov, G. Stoica, and L. V. Wang, Nature Biotechnol. **24,** 848 (2006).
12. L. Xiang, D. Xing, H. Gu, D. Yang, S. Yang, L. Zeng, and W. Chen, J. Biomed. Opt. **12,** 014001 (2007).
13. C. Zhang and Y. Wang, Acta Opt. Sin. (in Chinese) **28**, 2296 (2008).
14. E. W. Stein, K. Maslov, and L. V. Wang, J. Appl. Phys. **105,** 102027 (2009).
15. E. W. Stein, K. Maslov, and L. V. Wang, J. Biomed. Opt. **14,** 020502 (2009).
16. H. Guo and S. Yang, Rev. Sci. Instrum. **80,** 014903 (2009).
17. C. Passmann and H. Ermert, in *Proceedings of IEEE Ultrasonics Symposium* 1661 (1994).
18. C. Guittet, F. Ossant, L. Vaillant, and M. Berson, IEEE Trans. Biomed. Eng. **46,** 740 (1999).